https://doi.org/10.15302/J-LAF-0-020035 Received Date | 2024-10-15 Accepted Date | 2025-04-22

Simulation and Assessment of Rainstorm Flood Risk in Mountainous Rural Settlements Under Climate Change Scenarios

Zhe SUN[1,*], Yuwei JIA[1], Qijiang WU[1], Jiaxing JIANG[1], Lu ZHENG[1], Zixuan CUI[1], Luca Maria Francesco FABRIS[1,2]

1 School of Architecture and Urban Planning, Beijing University of Civil Engineering and Architecture, Beijing 100044, China
2 Department of Architecture and Urban Studies, Politecnico di Milano, Milano 20133, Italy

*CORRESPONDING AUTHOR
Address: No. 1, Zhanlanguan Road, Xicheng District, Beijing 100044, China
Email: sunzhe@bucea.edu.cn

GRAPHICAL ABSTRACT

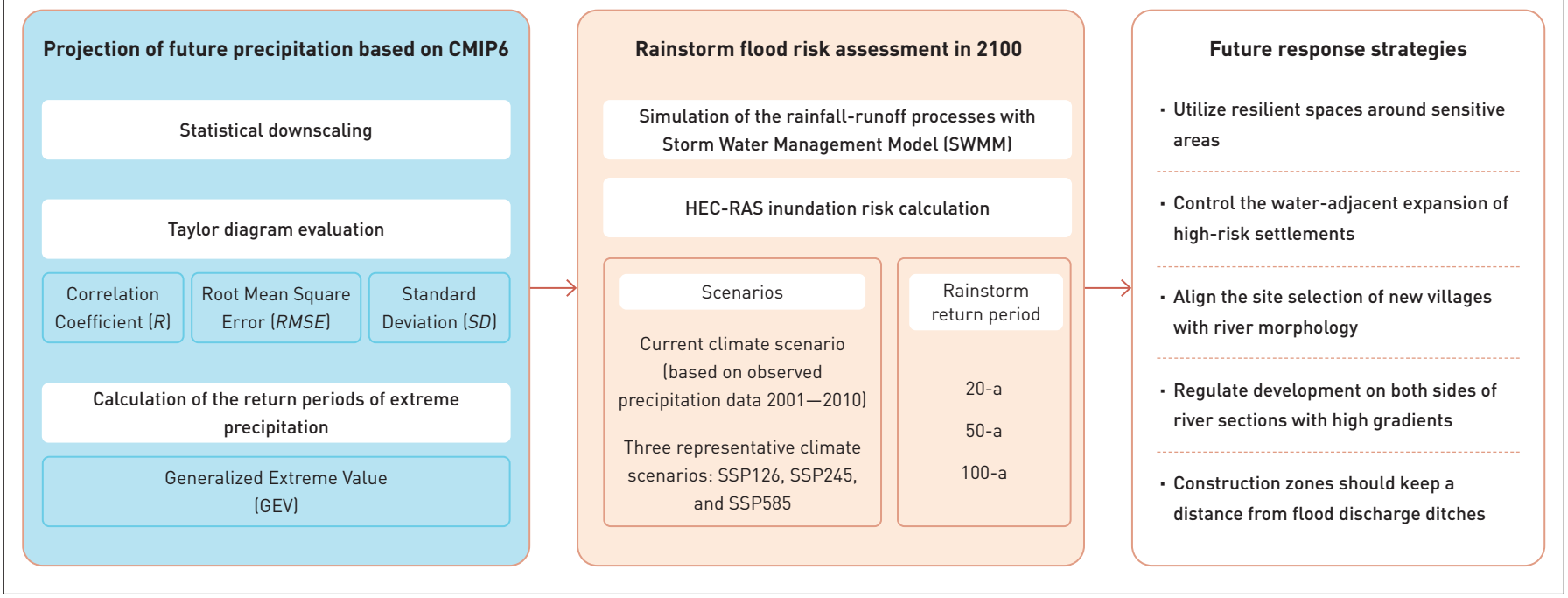

ABSTRACT

Climate change has significantly increased the intensity and frequency of extreme weather events, posing significant challenges to the hydrological ecological security of rural settlements in mountainous areas. There is an urgent need for research that predicts the flood risk of mountainous villages under future climate scenarios. Taking the mountainous area of the Yongding River Watershed in Beijing as an example, this study uses CMIP6 data and the Delta statistical downscaling method to predict precipitation with return periods of 20-a, 50-a, and 100-a under the SSP126, SSP245, and SSP585 scenarios at the end of this century. A two-dimensional hydrodynamic model combining SWMM and HEC-RAS has been employed to simulate the flood risks of the villages in the watershed. The results show that: 1) overall flood risk is higher for the villages located downstream of the Qingshui River and at the outlet of the Yongding River Gorge, with significantly increased inundation area ratio, maximum inundation depth, and the number of villages affected; 2) with the increase in radiative forcing values of the SSP pathways, the inundation area ratio increases by up to 8.22% by 2100, significantly increasing the flood control pressure on settlements in the future; 3) the correlation

results between village spatial characteristics and flood risks show that the inundation area ratio is significantly negatively correlated with average river width and river sinuosity, and significantly positively correlated with river gradient and floodway proximity; the maximum inundation depth is significantly negatively correlated with average river width and significantly positively correlated with floodway proximity. Finally, this research suggests that it is necessary to integrate various spatial elements and resources from upstream and downstream areas by prioritizing the strategy of key area flood control and sustainable development, to reduce the flood risk to mountainous settlements under future climate change.

KEYWORDS

Climate Change; CMIP6; Mountain Settlement; Flood Risk; Yongding River Watershed; Spatial Characteristic; Extreme Rainfall Event

HIGHLIGHTS

- Delta–GEV modeling projects flood risks for mountainous rural settlements by 2100 under future climate scenarios
- Extreme precipitation changes reveal escalating flood risks, with maximum inundation area ratio increases by 8.22%
- Spatial indicators of rural settlements quantify pluvial flood risks for resilience planning

RESEARCH FUNDS

- Project of "Research on the Mitigation Mechanism and Optimization Strategies of Urban Blue–Green Landscapes on the Heat Island Effect," Outstanding Young Talent Cultivation Program of the Beijing Municipal University Faculty Development Support Plan (No. BPHR202203082)
- Project of "Study on the Protection Experience of Historical Blocks and Ancient Villages and Towns With a Mixture of Old and New Elements," The National Social Science Fund of China (No. 24VWB022)
- Project of "Analysis and Application of the Mechanism of Flood Adaptation in Mountainous Traditional Settlements," The National Natural Science Foundation of China (No. 52478039)

EDITED BY Tina TIAN, Xidong MA

1 Introduction

The Intergovernmental Panel on Climate Change (IPCC) points out that climate change will increase the frequency and intensity of extreme meteorological events[1]. Mountains, however, are among the most vulnerable ecosystems affected by climate change, and are highly susceptible to extreme rainstorm events, which trigger disasters such as floods, debris flows, and landslides, as well as secondary disasters, resulting in significant losses[2]. The high occurrence of these disasters in mountainous areas is mainly due to their steep vertical gradients—the natural ecological characteristics are compressed horizontally, causing a more intense response of mountainous rainstorm processes to climate change compared with plains areas[3]. Moreover, the steep terrain and dense gullies in mountainous areas make short-period heavy rainfall prone to triggering flash floods and landslides, posing a high risk of river overflow to valley settlements[4–5]. Therefore, to address the climate challenges faced by mountainous rural settlements, it is urgent to advance research on future flood risk prediction, providing a scientific basis for their safety, resilience, and sustainable development.

Existing research on rural flood risk prediction and assessment is mainly conducted via two methods: the Characteristic Parameter Method and the Scenario Simulation Method. The former usually constructs characteristic parameters based on historical disaster data or flood-inducing factors and uses mathematical statistics such as weight overlay and machine learning for assessment[6]. For example, Samavia Rasool et al. integrated 65 indicators from physical, social, and institutional dimensions to build a composite index, and assessed the flood risk vulnerability of rural settlements in Pakistan through weighted calculations[7]; Meihong Ma et al. constructed a flood risk assessment system based on 13 hazardous indicators covering local meteorology, topography, and human activities, with an empirical study in Yunnan Province[8]; Qijiang Wu et al. combined multi-dimensional parameters such as settlement buffer zones, basin characteristics, and meteorological factors, and used the NSGA-II-GB multi-objective optimization algorithm to assess the spatial heterogeneity of flood risk in mountain settlements[9]. The research based on Scenario Simulation Method mainly relies on GIS and hydrodynamic modeling to dynamically assess risks by simulating flood inundation characteristics (e.g., duration, water depth, area) under different scenarios. Ranko Pudar et al. used the MODEL2014 to simulate and assess the design flood risks with return periods ranging from 2 a to 1,000 a in the Tamnava watershed in Serbia, and the

disaster losses of different mitigation strategies[10]; Po Yang et al.[11] and Weilin Wang et al.[12] both calculated the water surface profiles under different design flood peak flows or varied return period scenarios using hydrological models, and compared them with the elevations of riverside settlements to identify the risk levels and inundation water levels.

Most previous studies have focused on micro-scale simulations within single or several key settlements[13–14], lacking comparative simulation studies of different rural settlements at the small- to medium-sized watershed scales, especially predictions under future climate change scenarios[15]. Therefore, this study takes the Mentougou section of the Yongding River watershed in Beijing as an example and constructs a set of methods for simulating flood risks of small- to medium-sized watersheds with multiple settlements. This method simulates the flood risks of rural settlements within the watershed under various climate scenarios, accurately identifies the spatial differences in vulnerability, and aims to provide a scientific basis for developing targeted disaster prevention and mitigation strategies.

This study focuses on the following questions: 1) How to predict the flood risks of rural settlements within small- to medium-sized mountainous watershed under different climate scenarios? 2) What is the trend of the flood risks of mountainous rural settlements under different climate scenarios? And 3) how do the spatial characteristics of mountainous rural settlements affect the flood risk? By enhancing the ability to predict future flood risk of mountainous rural settlements, this study provides scientific and technological support for climate adaptation-oriented resilient planning and design.

2 Data Sources and Research Methods

2.1 Study Area

The study focuses on the Mentougou section of the Yongding River, which is a typical mountainous watershed in western Beijing. The mainstream flows from the Yanqing Basin through the Guanting Gorge into Mentougou District, with the Qingshui River tributary joining from the southwest. The total length of the river channel is 91.2 km. The steep mountains and narrow valleys along the mainstream accommodate numerous rural settlements[16]. Influenced by its geographical location and monsoon climate, the area often becomes a regional rainfall center[17]. In late July 2023, an extreme rainstorm occurred in the upper reaches, with the rainstorm center receiving over 600 mm of total precipitation and a maximum 24-hour rainfall of 348.3 mm. This led to a rapid rise in river levels and severe flooding (the "723 Rainstorm" hereafter)[18]. Given that future climate change is expected to intensify extreme weather events[19], the flood risk in mountainous rural settlements within this study area is largely growing, necessitating forward-looking multi-scenario flood simulations and analyses.

Considering the hydrological network structure, the distribution of water conservancy projects, and the layout of rural settlements, the simulation scope of this study covers 36 administrative villages located in the valley areas along the river downstream from the Zhaitang Reservoir, with a total area of 389.71 km^2 (Fig. 1). Among the 36 villages, 25 are adjacent to the mainstream of the Yongding River and 11 adjacent to the Qingshui River.

2.2 Data Sources

This study used two types of data: historical baseline data and CMIP6 multi-model data. The historical baseline precipitation data included datasets with different temporal resolutions: the 1-km-resolution monthly precipitation dataset of China (1901–2022) published by Shouzhang Peng[20] ("Dataset A" hereafter); the CN05.1 0.25°×0.25° resolution daily dataset of China (1961–2021), which was generated by interpolation data from over 2,400 observation stations throughout the country by Jia Wu et al.[21] ("Dataset B" hereafter); and historical hourly precipitation sequence data (from 00:00, July 29, 2023 to 23:00, August 2, 2023) derived from the European Centre for Medium-Range Weather Forecasts (ECMWF) dataset on the Xihe Energy Meteorological Big Data

Fig. 1 Study area (source: Beijing Municipal Commission of Planning and Natural Resources and Beijing Municipal Civil Affairs Bureau).

Platform, validated by the rainfall data from the Beijing Water Authority and used as precipitation input for the hydrological model ("Dataset C" hereafter). Additional historical baseline data comprised the DEM data sourced from the NASA Earth Science Data Systems (2020) with a resolution of 12.5 m; land-use data obtained from the Aerospace Information Research Institute of the Chinese Academy of Sciences with a resolution of 30 m; and observed river-discharge (flow) data provided by the Beijing Water Authority for the Sanjiadian Barrage and the Yanchi Hydrological Station (covering the corresponding period), which were used for model calibration/validation and for comparing simulated versus observed hydrographs. Drawing on previous research[22–24], the CMIP6 model data covered eight models that perform well in simulating precipitation in China, namely ACCESS-ESM1-5, BCC-CSM2-MR, CMCC-ESM2, INM-CM4-8, INM-CM5-0, IPSL-CM6A-LR, MIROC6, and NorESM2-MM.

This study selected three representative climate scenarios commonly used in academia—SSP126, SSP245, and SSP585—to predict the flood risk in the study area by 2100. These scenarios correspond to low, medium, and high levels of radiative forcing, with the stabilized radiative forcing values in 2100 being 2.6 W/m^2, 4.5 W/m^2, and 8.5 W/m^2, respectively.

2.3 Research Methods

This study aims to predict the flood risks of mountainous rural settlements under varied climate scenarios and analyze their relationships with settlement spatial characteristics. By downscaling climate data and predicting future extreme precipitation, future precipitation data were obtained as the input for subsequent hydrological and hydrodynamic simulations. Then, the inundation area ratio and maximum inundation depth of village settlements within the study area were calculated and used as key assessment indicators to identify high-risk areas and the specific flooding impacts among the villages. The study further analyzed the correlation between settlement spatial characteristic indicators and flood risk indicators to reveal the key spatial factors affecting settlement flood vulnerability.

2.3.1 Statistical Downscaling Method

Common climate downscaling methods include statistical downscaling, dynamical downscaling, and hybrid dynamical–statistical downscaling[25]. Statistical downscaling establishes quantitative relationships between large-scale climate fields and local observations for scale conversion, with the advantages of low computational resource requirements, diverse construction approaches, and relatively simple implementation. Dynamical downscaling relies on Regional Climate Models (RCMs) for high-resolution numerical simulations, enabling full description of physical processes. Hybrid dynamical–statistical downscaling attempts to combine the strengths of both methods. However, the latter two methods are often limited in practical applications due to high computational costs and complicated simulation configurations[26]. Given these considerations, this study selected the Delta statistical downscaling method recommended by the U.S. National Center for Atmospheric Research. This method sees advantages of low resource consumption and is relatively easy to implement, effectively reducing systematic biases between Global Climate Models (GCMs) and RCMs while retaining their variability characteristics under multiple scenarios, making it widely used in climate data downscaling research[27].

To address the spatial resolution differences between different climate models and observational data, and to enhance the accuracy of comparisons with observational data and the adaptability for regional climate studies, the climate model data of the study area were downscaled to a uniform spatial resolution of 1 km. The specific calculations are shown in Eqs. (1) and (2):

$$Bias_{\mathrm{month,cal}} = \frac{OBS_{\mathrm{month,cal}}}{GCM_{\mathrm{month,cal}}}, \tag{1}$$

$$GCM_{\mathrm{day,cor}} = GCM_{\mathrm{day,proj}} \times Bias_{\mathrm{month,cal}}, \tag{2}$$

where, $Bias_{\mathrm{month,cal}}$ is the calibration period scaling factor; $OBS_{\mathrm{month,cal}}$ is the multi-year monthly average of observational data during the calibration period; $GCM_{\mathrm{month,cal}}$ is the multi-year monthly average of the CMIP6 model data during the calibration period; $GCM_{\mathrm{day,proj}}$ is the daily precipitation from the CMIP6 model; and $GCM_{\mathrm{day,cor}}$ is the downscaled daily precipitation from the CMIP6 model.

The calibration period for downscaling in this study was selected from 1901 to 1984, and the evaluation period for downscaling effectiveness was from 1985 to 2014. To evaluate the downscaling effectiveness of daily observational precipitation data (Dataset B) and to screen for CMIP6 models with better simulation performance, three key indicators were used— Correlation Coefficient (R), Root Mean Square Error ($RMSE$), and Standard Deviation (SD)—and the results were visualized using Taylor diagrams.

2.3.2 Calculation Method for Extreme Precipitation Return Periods

The study employed the three-parameter Generalized Extreme Value (GEV) distribution function to determine the return periods of extreme precipitation. This method has been effectively applied

in related studies in the Beijing–Tianjin–Hebei region[28–30]. The extreme value distribution is a mathematical model that describes the probability characteristics of climate variable extremes. When the asymptotic distribution of sample extremes exists, it can be categorized into three types: Gumbel, Fréchet, and Weibull. In 1955, A. F. Jenkinson theoretically proved that these three distributions can be unified into a general GEV form. The cumulative distribution function and the probability density function are calculated as follows[31]:

$$F(x)=\begin{cases}\exp\left[-\left(1-k\times\dfrac{x-\beta}{\alpha}\right)^{\frac{1}{k}}\right], & k\neq 0\\ \exp\left[-\exp\left(-\dfrac{x-\beta}{\alpha}\right)\right], & k=0\end{cases}, \tag{3}$$

$$f(x)=\begin{cases}\dfrac{1}{\alpha}\exp\left[-\left(1+k\times\dfrac{x-\beta}{\alpha}\right)^{\frac{1}{k}}\right]\left(1+k\times\dfrac{x-\beta}{\alpha}\right)^{-1-\frac{1}{k}}, & k\neq 0\\ \dfrac{1}{\alpha}\exp\left[-\dfrac{x-\beta}{\alpha}-\exp\left(-\dfrac{x-\beta}{\alpha}\right)\right], & k=0\end{cases}. \tag{4}$$

In the equations, α, β, and k are the scale parameter, location parameter, and shape parameter, respectively. When $k = 0$, it is the Gumbel distribution; when $k > 0$, it is the Fréchet distribution; and when $k < 0$, it is the Weibull distribution.

2.3.3 Flood Risk Simulation and Analysis

2.3.3.1 Coupled Model Construction

The study employed the Storm Water Management Model (SWMM) to simulate the rainfall-runoff processes of sub-watersheds in the study area[32–34]. Based on the data of DEM, land use, and hourly precipitation sequences, GIS tools were used to delineate sub-watersheds, generalize river channels, and extract terrain information such as nodes. Key surface characteristic parameters of each sub-watershed were calculated, including area, slope, and characteristic width. The generalized river channel parameters were extracted and calculated, including length, cross-sectional geometric dimensions, maximum depth, roughness coefficient, and elevation offsets of upstream and downstream sections. The sub-watersheds and upstream river channels were connected to downstream river channels via nodes, constructing a one-dimensional coupled model of river networks and sub-watersheds. Subsequently, the Natural Breaks Method was applied to divide the study area into four zones with different precipitation levels from northwest to southeast. The average precipitation of each zone was calculated using the ArcGIS Raster Calculator.

The study designed the rainfall temporal distribution patterns according to the *Standard of Rainwater Runoff Calculation for Urban Storm Drainage System Planning and Design* (DB11/T969—2016) and calculated the future hourly precipitation sequence data. After inputting the data into the model, the flow hydrographs generated by the predicted precipitation events were obtained.

2.3.3.2 Model Accuracy Verification

The study utilized the Nash-Sutcliffe Efficiency (*NSE*) coefficient to calibrate the hydrological model by comparing the simulated flow data with the measured flow data observed from the 723 Rainstorm. The *NSE* is calculated as follows:

$$NSE = 1-\frac{\sum(Q_{obs}-Q_{sim})^2}{\sum(Q_{obs}-\bar{Q}_{obs})^2}, \tag{5}$$

where Q_{sim} represents the simulated flow; Q_{obs} represents the observed flow, and $\bar{Q}_{obs}$ represents the average of all observed flows. The closer the *NSE* value is to 1, the better the fit between the simulated results and the observations, indicating higher model accuracy. According to the classification criteria proposed by Daniel N. Moriasi, *NSE* values are divided into four levels: excellent (> 0.7), good (0.6 ~ 0.7), satisfactory (0.5 ~ 0.6), unsatisfactory (≤ 0.5). This provides a reference for setting reliability thresholds in practical applications[35].

Subsequently, by comparing the simulated inundation area with the actual inundation area, the accuracy of the river simulation system (HEC-RAS) model has been verified using the Critical Success Index (*CSI*)[36]. The formula for calculating the *CSI* is as follows:

$$CSI = \frac{A_{obs}\cap A_{mod}}{A_{obs}\cup A_{mod}}, \tag{6}$$

where A_{obs} and A_{mod} represent the areas of the actual and simulated inundation extents, respectively. When the simulated area and the observed area are completely overlapped, the *CSI* equals 1; when there is no overlap, the *CSI* is 0. Therefore, the closer the *CSI* is to 1, the larger the overlap area, indicating higher accuracy of the simulation results.

2.3.3.3 Inundation Risk Calculation

The study employed HEC-RAS to construct the terrain of the study area and set the hydrological boundary conditions, simulating the rainfall-runoff process and extracting the maximum inundation extent. Based on these results, the study calculated the inundation area ratio and maximum inundation depth of the settlements to assess the impact levels of floods.

2.3.4 Calculation of the Spatial Characteristic Indicators of Villages

The study selected the spatial characteristic indicators of villages from three dimensions: topography, hydrology, and settlement (Table 1). GIS spatial analysis techniques were used to obtain the corresponding data, and the Spearman correlation coefficient was employed to explore their correlations with the flood risks of settlements.

Table 1: Spatial characteristic indicators of villages and calculation methods

Dimension	Indicator	Calculation method	Definition and explanation
Topography	Average slope	SP	The average slope of the DEM grid cells within a given village
	Topographic relief	$RF = H_{max} - H_{min}$	The difference between the maximum and minimum elevations in a given village
Hydrology	Average river width	$W = A_R/D$	The ratio of river area A_R to river length D within a given village
	River sinuosity	$C = D/D_0$	The ratio of river length D to the straight-line distance D_0 between river ends
	River gradient	$R = \triangle H/D$	The ratio of elevation difference $\triangle H$ to river length D within a given village
	Floodway proximity	T	The presence of a floodway adjacent to a given village
Settlement	Settlement size	A	The area of a given settlement
	Settlement shape	$\lambda = l/b$	The ratio of the length l to the width b of the bounding rectangle of a given settlement

3 Research Results

3.1 Downscaling Effectiveness Evaluation

The performance improvement of each model after downscaling is shown in Table 2 and Fig. 2. In Fig. 2, the concentric circles and

Table 2: Comparison of the simulation performance among different models after downscaling

Rank	Model	*R*		*RMSE* (mm/month)		*SD*	
		Pre	Post	Pre	Post	Pre	Post
	Observation	1	—	0	—	27.72	—
1	Dataset B	0.95	0.96	15.49	11.44	38.23	34.59
2	ACCESS-ESM1-5	0.94	0.94	23.39	12.15	41.96	33.81
3	INM-CM4-8	0.94	0.95	40.62	12.14	48.56	34.38
4	NorESM2-MM	0.95	0.97	31.23	13.40	50.66	37.47
5	CMCC-ESM2	0.95	0.93	48.33	13.73	58.25	34.81
6	IPSL-CM6A-LR	0.92	0.95	32.14	16.42	48.50	39.16
7	BCC-CSM2-MR	0.91	0.90	19.87	18.32	38.88	38.53
8	MIROC6	0.90	0.91	51.01	18.10	58.22	38.53
9	INM-CM5-0	0.94	0.93	57.60	21.28	60.05	43.15

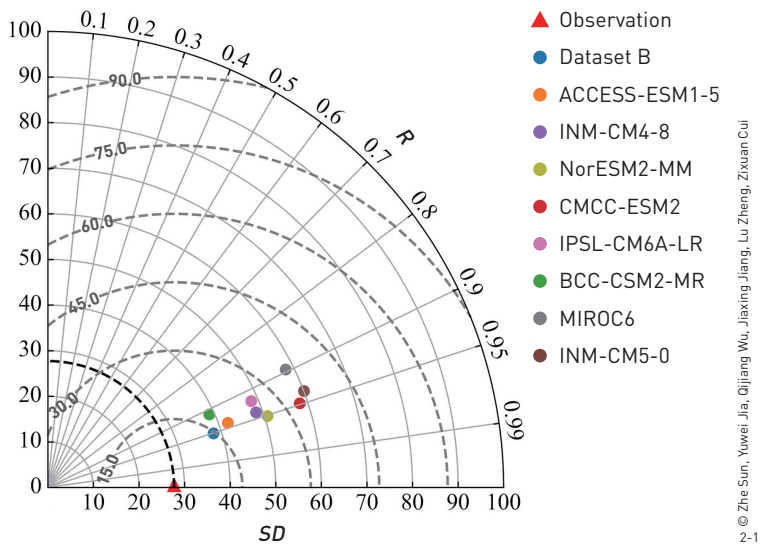

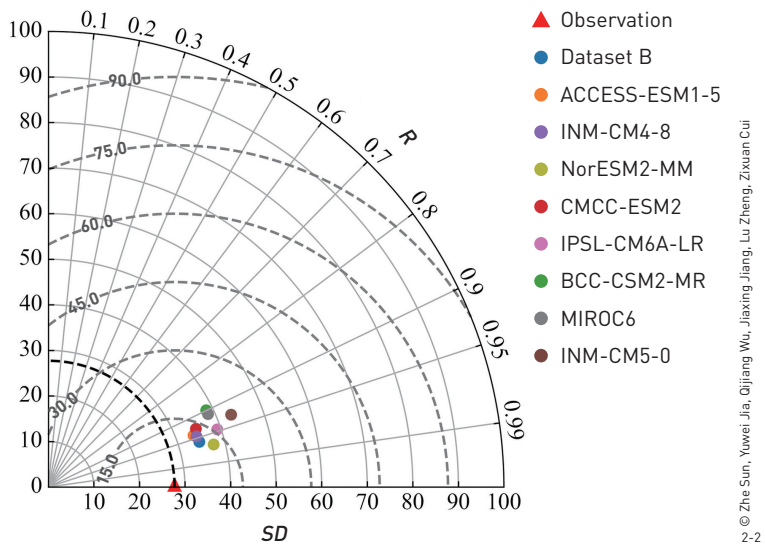

Fig. 2-1 Taylor diagram before downscaling.
Fig. 2-2 Taylor diagram after downscaling.

coordinate axes represent the ratio of the *SD* of the simulated results to the observed results, while the corresponding *R* value is represented by the radial coordinate. Meanwhile, the *RMSE* is indicated by the distance between the observed and simulated results—the smaller the value, the closer the simulation is to the observation[37].

The results show that after downscaling, the *R* value of Dataset B increased to 0.96, the *RMSE* decreased to 11.44, and the *SD* was 34.59, indicating a high degree of consistency between the simulated precipitation and the observed data. Among the CMIP6 models, NorESM2-MM had the highest *R* value of 0.97, INM-CM4-8 had the smallest *RMSE* of 12.14, and ACCESS-ESM1-5 had the *SD* (33.81) closest to the value of Dataset B (34.59), with the best simulation performance. To select the optimal model, the study used the entropy-weighted TOPSIS method to rank the three indicators[23–24]. Overall, ACCESS-ESM1-5 performed best after downscaling (*R* = 0.94, *RMSE* = 12.15, *SD* = 33.81), and its downscaled results were selected for subsequent analyses.

3.2 Evaluation of Model Validation Results

The study calibrated the SWMM parameters based on rainfall-runoff process data (Dataset C as precipitation input) and further optimized the parameters using the monitored flow (river-discharge) data provided by the Beijing Water Authority at the Sanjiadian Barrage and the Yanchi Hydrological Station, so as to compare the simulated and observed rainfall-runoff processes (Fig. 3). The *NSE* coefficients for the rainfall-runoff processes at the Sanjiadian Barrage and Yanchi Hydrological Station were 0.67 and 0.75, respectively, indicating that the SWMM can accurately simulate the rainfall-runoff process in the study area.

The simulated inundation area largely overlapped with the observed inundation area (Fig. 4) and the *CSI* for the studied river section was 0.67, further verifying that the model has good accuracy in simulating the inundation area.

3.3 Flood Risk Analysis of Village Settlements

3.3.1 Identification of Key Flood Risk Areas

The inundation simulation results under the current climate scenario (Fig. 5) show that the overall flood risk of the study area decreases from the northwest to the center and then increases towards the southeast. High-risk areas are concentrated on both sides of the riverbanks in Zhaitang Town, Wangping Town,

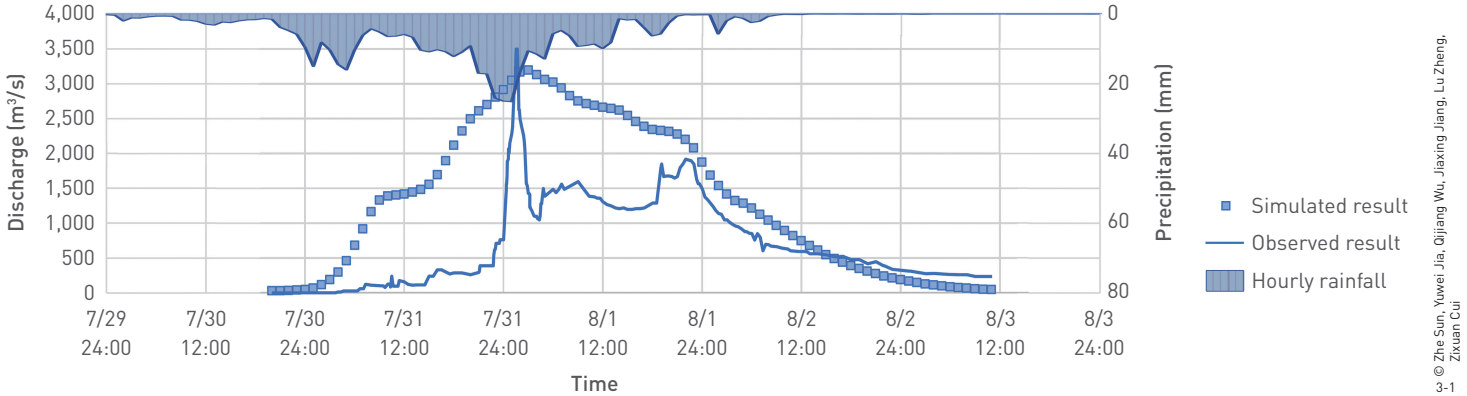

3-1

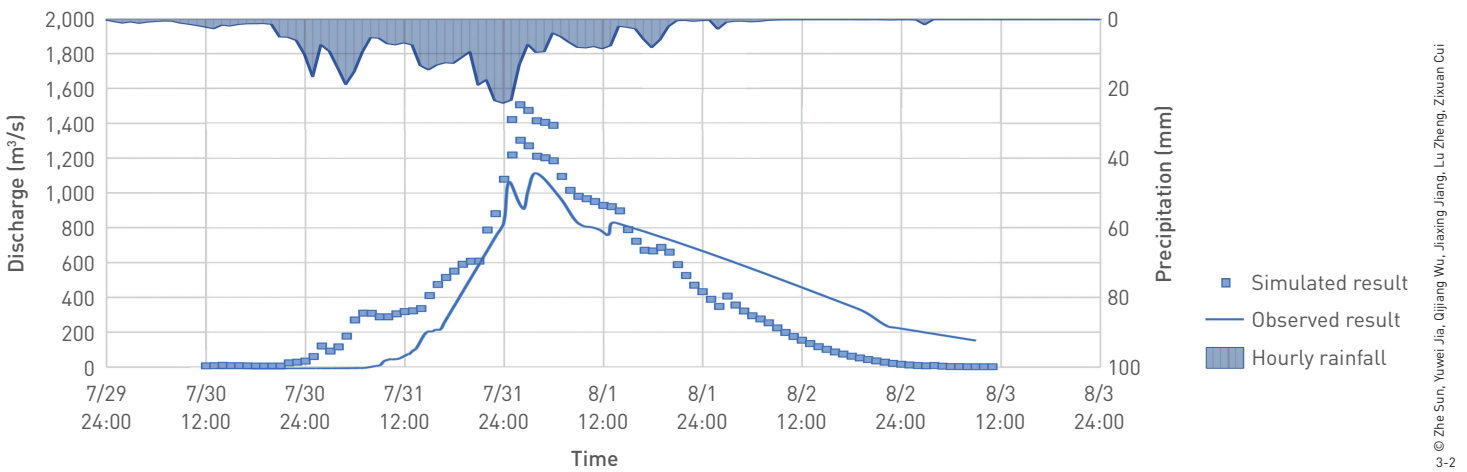

3-2

Fig. 3 Validation flow process results of the SWMM model at the Sanjiadian Barrage (Fig. 3-1) and at the Yanchi Observation Station (Fig. 3-2).

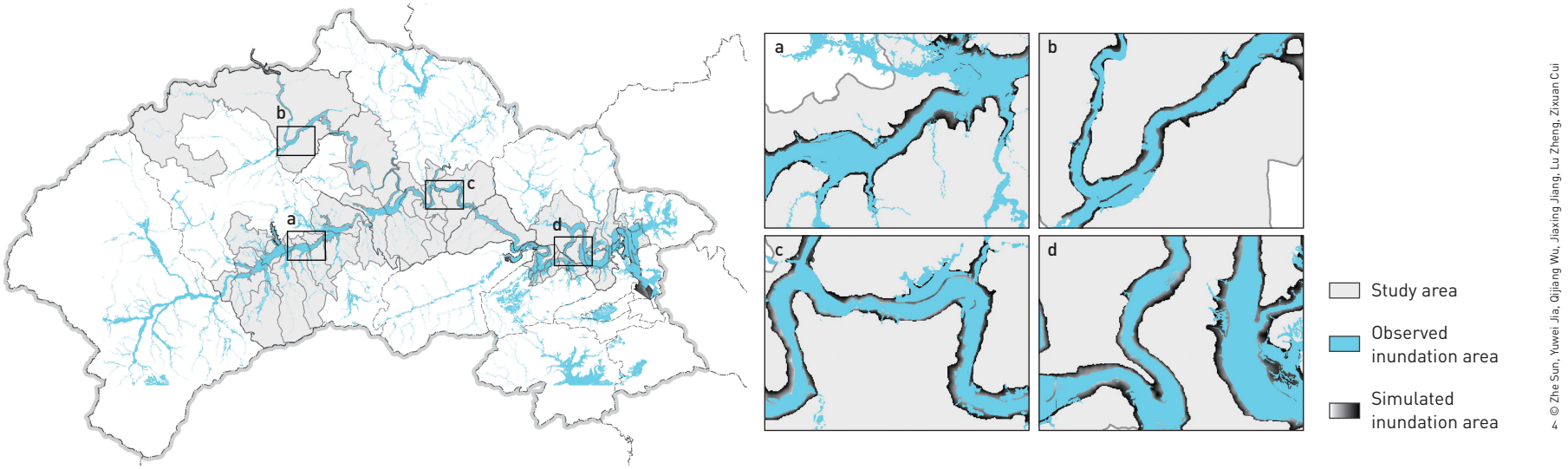

Fig. 4 Comparison of HEC-RAS observed inundation area and simulated inundation area (source: Beijing Municipal Commission of Planning and Natural Resources and Beijing Municipal Civil Affairs Bureau).

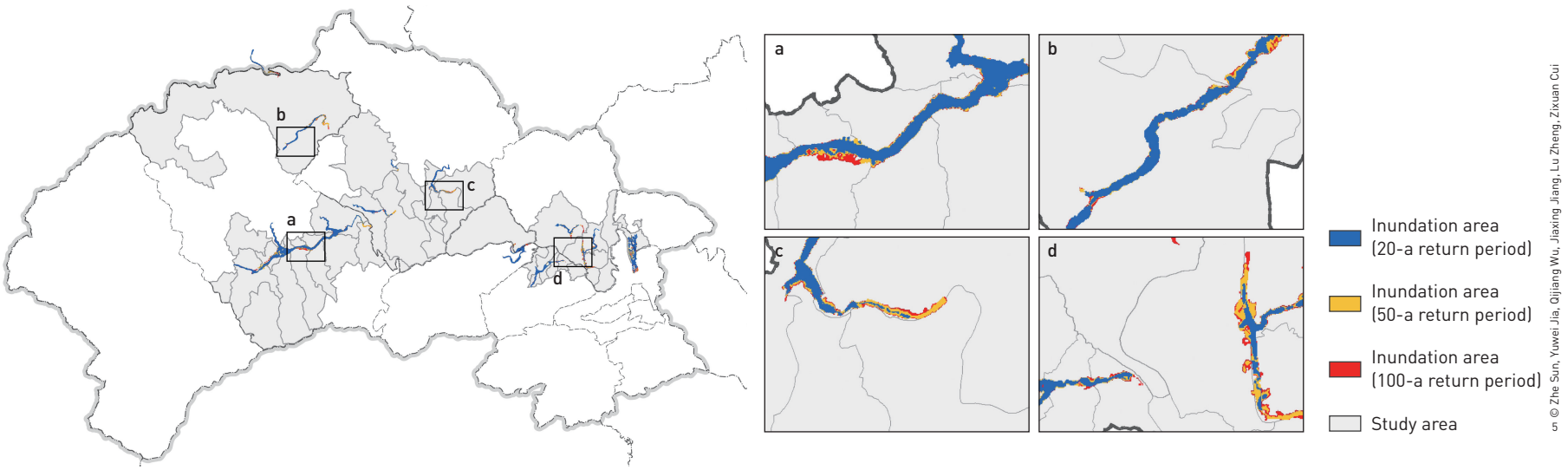

Fig. 5 Analysis of inundation area across different return periods (2001–2010) (source: Beijing Municipal Commission of Planning and Natural Resources and Beijing Municipal Civil Affairs Bureau).

Miaofengshan Town, and Junzhuang Town, while the risk in Yanchi Town is relatively low.

Using the Natural Breaks Method, the overall inundation area ratio of villages was divided into four risk levels: low (0), moderate (0, 50%], high (50%, 75%], and extremely high (75%, 100%] (Fig. 6). The villages of higher flood risk are mostly located downstream of the Qingshui River and at the outlet of the Yongding River Gorge. Analyses under different return periods indicate that: 1) For the 20-a return period, the inundation area ratios of Gaopu Village, Nanjian Village, and Sangyu Village exceed 50%, with Nanjian Village being the most severely at 83.1%; 2) For the 50-a return period, Donghulin Village and Junxiang Village are added to the list of villages with inundation area ratios above 50%, and Gaopu Village has the highest risk with the inundation area ratio of 83.4%; And 3) for the 100-a return period, the number of villages with inundation area ratios exceeding 50% remains unchanged compared with the 50-a return period scenario, and Gaopu Village still exhibits the highest risk with the inundation area ratio rising to 84.9%. These findings indicate that villages adjacent to the Qingshui River suffer more severe flooding impacts, which are mostly located close to the riverbanks or along the confluence channels, making them most vulnerable during extreme rainfall events.

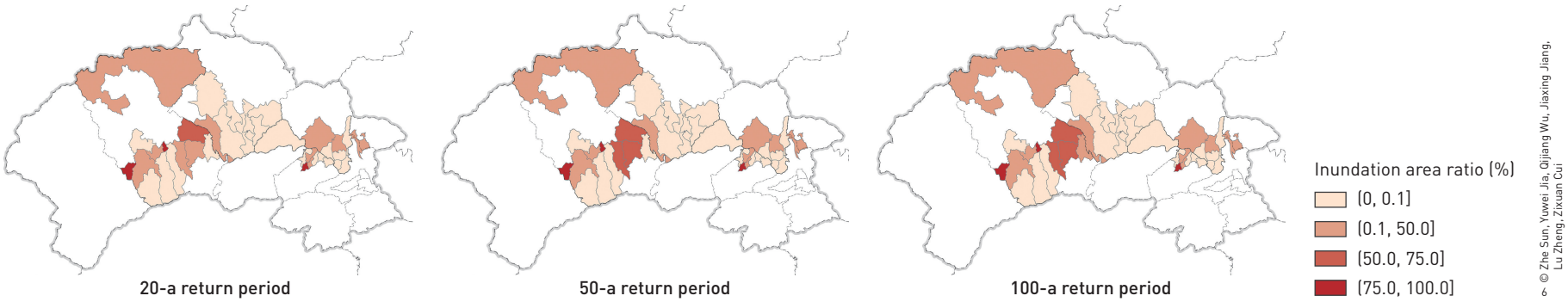

Fig. 6 Analysis of village inundation area across different return periods (2001–2010) (source: Beijing Municipal Commission of Planning and Natural Resources and Beijing Municipal Civil Affairs Bureau).

3.3.2 Analysis of Inundation Area Under Varied Future Climate Scenarios

The comparison results under the current climate scenario and the SSP126, SSP245, and SSP585 scenarios (Fig. 7) show that the inundation area ratio of village settlements increases under varied future climate scenarios, with the flood risks escalating due to extreme precipitation. Under the current climate scenario, the inundation areas caused by 20-a, 50-a, and 100-a return period rainstorms are approximately 65.96 hm^2, 71.19 hm^2, and 76.18 hm^2, respectively. By 2100, under the SSP126 scenario, the inundation areas increase to approximately 86.9 hm^2, 97.8 hm^2, and 104.5 hm^2, respectively; under the SSP245 scenario, they are approximately 65.96 hm^2, 92.9 hm^2, and 101.4 hm^2, respectively; and under the SSP585 scenario, they significantly rise to 102 hm^2, 109.9 hm^2, and 118.9 hm^2, respectively.

By the end of the century, under the three scenarios, the maximum increase in inundation area ratio will increase by 8.22% (Fig. 7). The zones with increased flood risk are primarily distributed along the middle river section in Zhaitang Town and the eastern river section in Miaofengshan Town (Fig. 8), with slight spatial variations under different scenarios.

Fig. 7 Analyses of inundation area ratio under current climate scenario and three future climate scenarios.

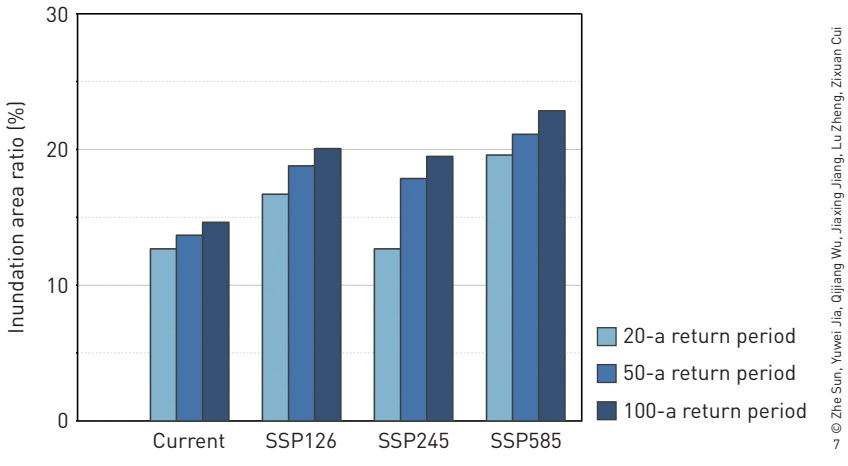

1) SSP126 scenario: For the 20-a return period, the inundation risk areas are located in the middle part of Zhaitang Town, the southeast of Wangping Town, and the west of Junzhuang Town; For the 50-a return period, the inundation risk area expands to the confluence of the Qingshui River at the borders between Zhaitang Town and Yanchi Town, as well as the eastern river section in Miaofengshan Town; For the 100-a return period, the risk area further extends to the middle river section in Yanxi Town and the northwest river section in Wangping Town.

2) SSP245 scenario: The inundation risk area for the 100-a return period significantly enlarges, particularly along the eastern river section in Miaofengshan Town. Under this scenario, climate change intensifies the impact of high-return period precipitation, where heavy rainfall events tend to accumulate into flood peaks in the flat river channels with low, gentle, and wide banks in Miaofengshan Town, inundating villages around the downstream outlet.

3) SSP585 scenario: The inundation risk area for the 20-a return period shows a notable increase but remains concentrated in the middle part of Zhaitang Town and the eastern part of Miaofengshan Town. This indicates that under this scenario, climate change will bring a more pronounced impact on short-return period rainfall events.

3.4 Correlations Between Village Spatial Characteristics and Extreme Flood Risks

3.4.1 Correlations Between Single-Dimension Village Spatial Characteristics and Extreme Flood Risks

This study selected the flood inundation area under the

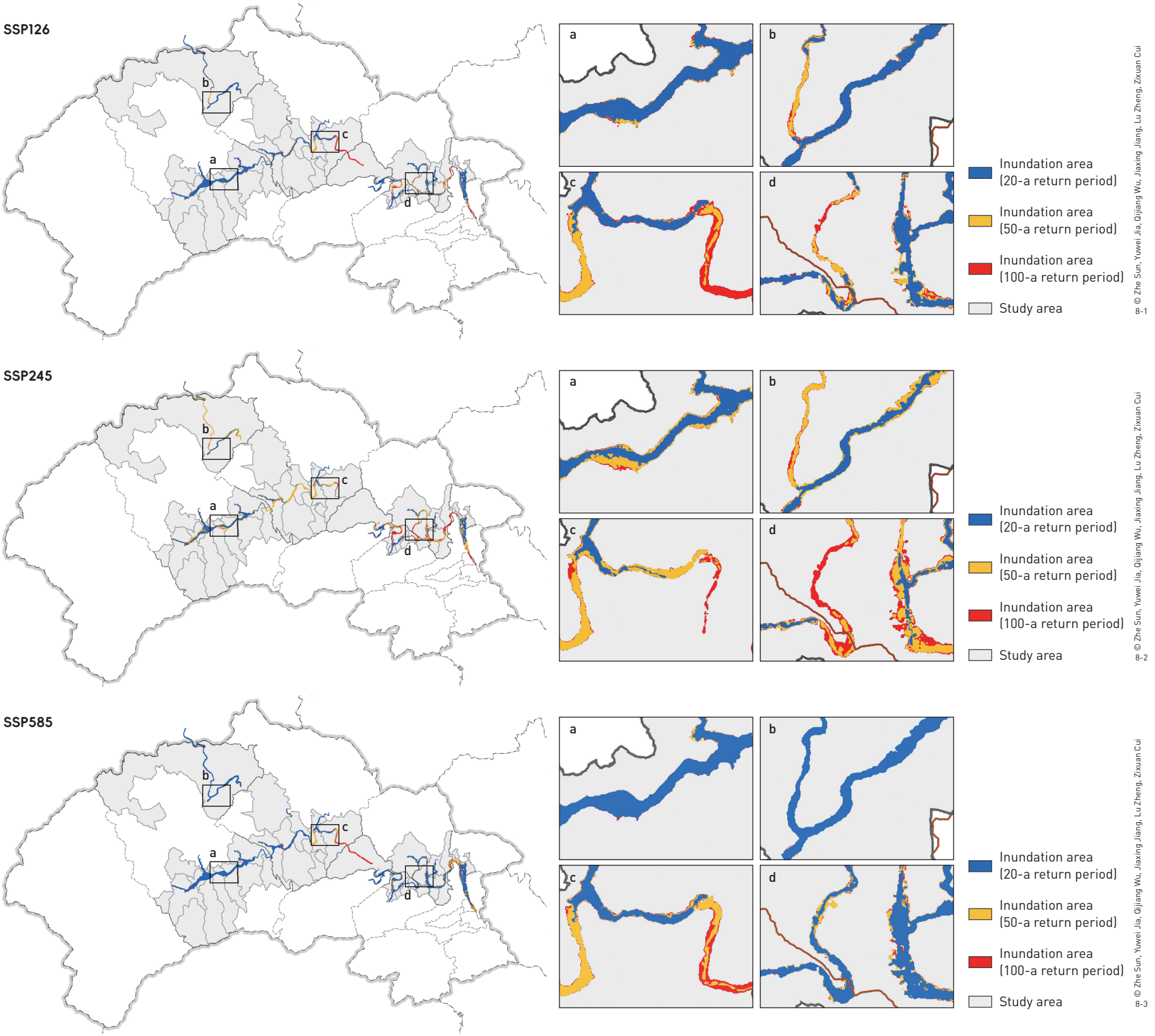

Fig. 8 Projected rainfall-runoff inundation area under three scenarios by 2100 (source: Beijing Municipal Commission of Planning and Natural Resources and Beijing Municipal Civil Affairs Bureau).

SSP585 scenario by 2100 with a 100-a return period to represent extreme flood risk and analyzed its correlations with village spatial characteristics. The Shapiro-Wilk test results showed that the W-statistics for the inundation area ratio and the maximum inundation depth were 0.810 ($p < 0.05$) and 0.922 ($p < 0.05$), respectively, indicating non-normal distributions. Therefore, the

Spearman correlation analysis was performed by examining the correlations between extreme flood risk indicators (the inundation area ratio and the maximum inundation depth) with the topographic, hydrological, and settlement characteristics of the villages.

The results (Table 3) showed that there was no significant correlation between the flood risk and the topographic and settlement characteristics, but a significant correlation with the hydrological characteristics. The average river width ($p < 0.01$) and river sinuosity ($p < 0.01$) were significantly negatively correlated with the inundation area ratio; the average river width was significantly negatively correlated with the maximum inundation depth ($p < 0.01$). The floodway proximity was significantly positively correlated with both the inundation area ratio ($p < 0.001$) and the maximum inundation depth ($p < 0.05$). The river gradient was significantly positively correlated with the inundation area ratio ($p < 0.01$).

Specifically, an increase in the average river width can expand the cross-section for water flows and enhance the flood discharge capacity. For example, in the downstream of the Yongding River, villages such as Shuiyuzui and Dongwangping had an average river width of over 250 m, and their inundation area ratios remained below 10% and the maximum inundation depths were under 1.1 m. An increase in river sinuosity can enhance flood detention and peak reduction, slow down the flow velocity, thereby reducing the flood risk. For example, Fujiatai Village, located at a meandering section of the Yongding River, had a river sinuosity greater than 2 and an inundation area ratio less than 1%. However, due to the limited cross-section for water flows, the floodway in the village would face a significant pressure in flood discharge during extreme rainfall events, leading to a higher risk of flood overflow.

Table 3: Analysis results of the correlations between single-dimension village spatial characteristics and extreme flood risks

Dimension	Indicator	Inundation area ratio		Maximum inundation depth	
		R	*p*	*R*	*p*
Topography	Average slope	−0.045177	0.822950	0.076923	0.702939
	Topographic relief	−0.100122	0.619271	−0.002442	0.990355
Hydrology	Average river width	−0.541928**	0.003502	−0.585917**	0.001321
	River sinuosity	−0.507786**	0.006853	−0.198168	0.321755
	River gradient	0.526493**	0.004785	0.258055	0.193743
	Floodway proximity	0.606199***	0.000804	0.434634*	0.023482
Settlement	Settlement size	−0.008547	0.966251	0.091575	0.649628
	Settlement shape	0.021368	0.915751	0.076313	0.705192

NOTE
* means $p < 0.05$; ** means $p < 0.01$; and *** means $p < 0.001$.

3.4.2 Correlations Between Overall Village Spatial Characteristics and Extreme Flood Risks

The study mapped the normalized village spatial characteristics of the studied villages onto extreme flood risk coordinate diagrams (Fig. 9) with the inundation area ratio as the horizontal axis and the maximum inundation depth as the vertical axis. The position in the coordinates of the center point of the radar chart for each village represents its estimated flood risk.

The results showed that among topographic characteristics, villages with higher topographic relief tended to have larger inundation area ratios, while those with greater average slope tended to have higher maximum inundation depths. Regarding hydrological characteristics, villages with a higher river sinuosity (single-peak in river sinuosity), such as Shuiyuzui and Longjiazhuang, had smaller inundation area ratios and lower maximum inundation depths. In contrast, villages with proximity to floodways and larger average river widths (multi-peak in river sinuosity), like Gaopu and Sangyu, had greater flood risks for both indicators. Among settlement characteristics, villages with a higher shape index or tending towards a linear shape (single-peak in river sinuosity), such as Yanhecheng, exhibited lower inundation area ratios but higher maximum inundation depths, suggesting risks of local severe floods. This is primarily due to the fact that the spatial distribution presents a linear layout along the river course reducing the affected area, while the elevation differences lead to deeper water accumulation in lower-lying settlements.

4 Conclusions and Discussion

This research, based on the CMIP multi-model datasets and long-term meteorological observation data, used the Delta statistical downscaling method and the Taylor diagrams to simulate the flood

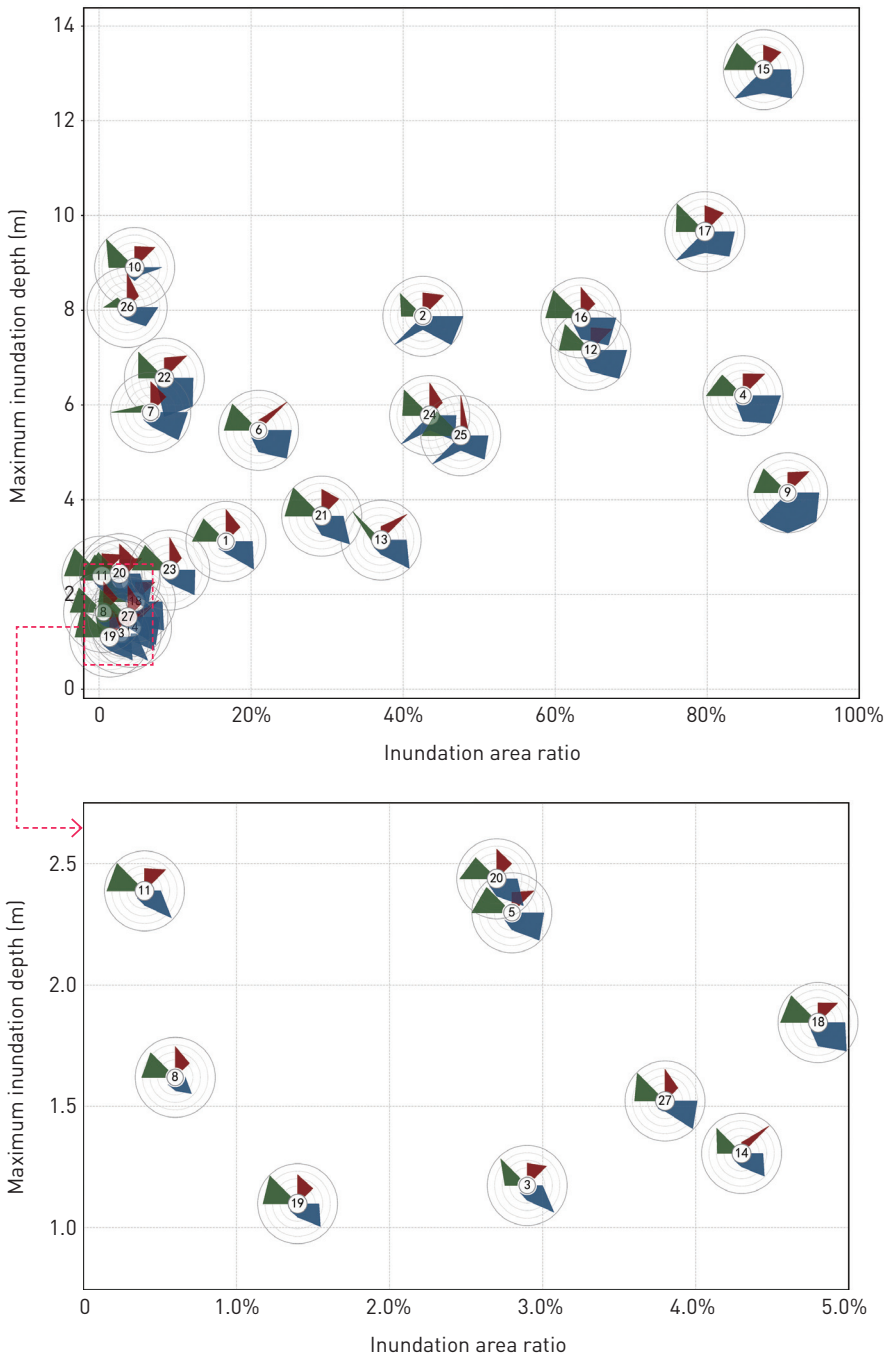

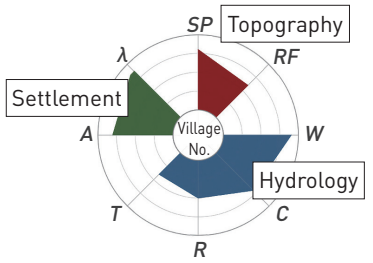

① Chenjiazhuang Village
② Danli Village
③ Dingjiatan Village
④ Donghulin Village
⑤ Dongshiguyan Village
⑥ Dongzhaitang Village
⑦ Facheng Village
⑧ Fujitai Village
⑨ Gaopu Village
⑩ Hebei Village
⑪ Jiuyuan Village
⑫ Junxiang Village
⑬ Junzhuang Village
⑭ Longjiazhuang Village
⑮ Nanjian Village
⑯ Qingbaikou Village
⑰ Sangyu Village
⑱ Seshufen Village
⑲ Shuiyuzui Village
⑳ Taizimu Village
㉑ Xihulin Village
㉒ Xizhaitang Village
㉓ Xiamaling Village
㉔ Xiaweidian Village
㉕ Xiangyangkou Village
㉖ Yanhecheng Village
㉗ Yanchi Village

Fig. 9 Extreme flood risk estimation of the villages in the study area.

risks of mountainous rural settlements with 20-a, 50-a, and 100-a return periods under the SSP126, SSP245, and SSP585 scenarios by the end of the century, focusing on the Mentougou section of the Yongding River Watershed in Beijing. The study systematically evaluated the differences in flood risks of the mountainous settlements in the study area and revealed the impact mechanisms of village spatial characteristics in topography, hydrology, and settlements on inundation risks.

The main findings of this research included that 1) the overall flood risk of the study area will increase significantly under varied future climate scenarios, with an increase of 8.22% in the inundation area ratio for the 100-a return period under the SSP585 scenario compared with the current situation; 2) the inundation area ratio was significantly negatively correlated with average river width and river sinuosity, and significantly positively correlated with river gradient and floodway proximity; and 3) the maximum inundation depth was significantly negatively correlated with average river width and significantly positively correlated with floodway proximity.

The above findings provide an important scientific basis for the resilience planning of mountainous rural areas. For high flood risk areas, such as the downstream of the Qingshui River

and the Yongding River Gorge, it is necessary to strengthen rigid defence measures and joint scheduling of reservoirs and to build flood control zones by linking surrounding resilient spaces. For settlements with extremely high inundation area ratios (exceeding 75%), such as Gaopu Village and Nanjian Village, it is recommended to implement relocation to areas above the elevation of the 100-a flood level, construction of flood embankments, and maintenance of river buffer zones, and to strictly control the disorderly cross-river expansion of high-risk settlements. For future sustainable development and construction, settlement sites should fully consider river morphology and avoid narrow floodplain plains and strictly adhere to the river blue-line construction standards; ecological protection zones should be added on the concave riverbanks to mitigate the impact of water flows, reduce the development intensity of high-gradient river sections, and ensure the safety distance of mountain flood discharge channels. This integrated strategy, which prioritizes key area flood control with sustainable development, can effectively reduce the flood risk caused by future climate change through upstream–downstream coordinated management of the spatial elements and resources[38].

There are two limitations in this study. First, the simulation accuracy of the model used in this study for complex mountainous characteristics such as topographic relief and geological structure was insufficient, resulting in certain deviations between the simulation results of the rainfall-runoff processes and the actual situations. Second, the simulation study did not consider the superposition impact of secondary disasters such as landslides and debris flows, which may underestimate the disaster risk intensity in certain areas.

审图号：GS京（2025）1690号

Competing interests | The authors declare that they have no competing interests.

REFERENCES

[1] Academy of Disaster Reduction and Emergency Management (ADREM), Ministry of Emergency Management & Ministry of Education, & China Association for Disaster Prevention. (2025). Global disaster data platform [Data set]. *Global Disaster Data Platform*.

[2] Adler, C., Wester, P., Bhatt, I., Huggel, C., Insarov, G. E., Morecroft, M. D., …, & Prakash, A. (2022). Cross-Chapter Paper 5: Mountains. In: H.-O. Pörtner, D. C. Roberts, M. Tignor, E. S. Poloczanska, K. Mintenbeck, A. Alegría, … & B. Rama (Eds.), *Climate Change 2022: Impacts, Adaptation and Vulnerability: Contribution of Working Group II to the Sixth Assessment Report of the Intergovernmental Panel on Climate Change*. Cambridge University Press.

[3] Lu, W., Tang, J., Zhang, X., Liu, H., & Luo, Z. (2020). Hydrological simulation in mountainous region: Present state and perspectives. *Mountain Research*, *38*(1), 50–61.

[4] Ma, J., Gao, H., & Xu, C. (2024). Characteristics of flash flood-debris flow disaster induced by the '23·7' rainstorm in Hantai Village, Changping District, Beijing. *Water Resources and Hydropower Engineering*, *55*(7), 1–18.

[5] Wang, X., Wang, Y., Lin, Q., Li, N., Zhang, X., & Zhou, X. (2022). Projection of China landslide disasters population risk under climate change. *Climate Change Research*, *18*(2), 166–176.

[6] Li, C., Tian, J., & Shen, R. (2020). Review on assessment of flood and waterlogging risk. *Journal of Catastrophology*, *35*(3), 131–136.

[7] Rasool, S., Rana, I. A., & Waseem, H. B. (2024). Assessing multidimensional vulnerability of rural areas to flooding: An index-based approach. *International Journal of Disaster Risk Science, 15*(1), 88–106.

[8] Ma, M., Zhao, G., He, B., Li, Q., Dong, H., Wang, S., & Wang, Z. (2021). XGBoost-based method for flash flood risk assessment. *Journal of Hydrology*, *598*, 126382.

[9] Wu, Q., Sun, Z., Wang, Z., Zheng, L., Jiang, J., Zhong, Z., & Jia, Y. (2025). Flood risk in mountainous settlements: A new framework based on an interpretable NSGA-II-GB from a point-area duality perspective. *Journal of Environmental Management*, *373*, 123842.

[10] Pudar, R., Plavšić, J., & Todorović, A. (2020). Evaluation of green and grey flood mitigation measures in rural watersheds. *Applied Sciences*, *10*(19), 6913.

[11] Yang, P., Wei, B., Li, X., & Yang, M. (2018). Study on the quantitative division of dangerous areas of flood disasters along the river villages. *Journal of Natural Disasters*, *27*(3), 130–135.

[12] Wang, W., Gu, S., Sang, G., Li, Q., Song, S., Zheng, C., & Wang, H. (2020). Disaster level and dangerous zone division in flood disaster along with river villages in hilly areas. *South-to-North Water Transfers and Water Science & Technology*, *18*(3), 119–126.

[13] Zhen, Y., Liu, S., Zhong, G., Zhou, Z., Liang, J., Zheng, W., & Fang, Q. (2022). Risk assessment of flash flood to buildings using an indicator-based methodology: A case study of mountainous rural settlements in Southwest China. *Frontiers in Environmental Science*, *10*, 931029.

[14] Ongdas, N., Akiyanova, F., Karakulov, Y., Muratbayeva, A., & Zinabdin, N. (2020). Application of HEC-RAS (2D) for flood hazard maps generation for

Yesil (Ishim) River in Kazakhstan. *Water*, *12*(10), 2672.
[15] Li, C., Sun, N., Lu, Y., Guo, B., Wang, Y., Sun, X., & Yao, Y. (2022). Review on urban flood risk assessment. *Sustainability*, *15*(1), 765.
[16] Lu, S., Pan, J., Li, C., & Sun, Z. (2023). Optimization of Watershed Landscape Pattern Based on Bird Habitat Connectivity: Taking the Yongding River Basin (Mentougou Section) as An Example. In: *Proceedings of the 2023 China Urban Planning Annual Conference: People's City, Planning Empowers—08 Urban Ecological Planning* (pp. 559–568). Beijing University of Civil Engineering and Architecture.
[17] Wu, Q., Guo, H., Yang, B., & Sun, J. (2009). Effects of topography and urban heat circulation on a Meso-β torrential rain in Beijing Area. *Meteorological Monthly*, *35*(12), 58–64, 164.
[18] Ren, S., & Wang, T. (2023). Beijing: Torrential rainstorms left about 77% of the population in Mentougou District affected, and 40 villages need reconstruction. *Beijing Daily*.
[19] Yu, K. (2021). Climate adaptation and resilience. *Landscape Architecture Frontiers*, *9*(6), 4–7.
[20] Peng, S., Ding, Y., Liu, W., & Li, Z. (2019). 1 km monthly temperature and precipitation dataset for China from 1901 to 2017. *Earth System Science Data*, *11*(4), 1931–1946.
[21] Wu, J., & Gao, X. (2013). A gridded daily observation dataset over China region and comparison with the other datasets. *Chinese Journal of Geophysics*, *56*(4), 1102–1111.
[22] Wu, H., Qin, Y., Xie, C., & Che, S. (2023). Spatial-temporal pattern evaluation and planning solution of urban flood risk in Shanghai based on CMIP6. *Chinese Landscape Architecture*, *39*(6), 26–32.
[23] Chang, S., Qu, Z., Wang, B., Su, Y., & Wang, J. (2023). Prediction of future down-scaled summer precipitation in Liaoning based on CMIP6 models. *Henan Science*, *41*(10), 1469–1478.
[24] Lin, W., Chen, H., Xu, H., Ai, Y., He, W., Zhang, D., Wang, F., Bi, W., & Wang, W. (2023). Significant increase of precipitation extremes will enlarge its population exposure over Southwest China in the future. *Transactions of Atmospheric Sciences*, *46*(4), 499–516.
[25] Xu, Z., Han, Y., & Yang, Z. (2019). Dynamical downscaling of regional climate: A review of methods and limitations. *Scientia Sinica Terrae*, *49*(3), 487–498.
[26] Liu, Y., Guo, W., Feng, J., & Zhang, K. (2011). A summary of methods for statistical downscaling of meteorological data. *Advances in Earth Science*, *26*(8), 837–841.
[27] Zhao, F., & Xu, Z. (2007). Comparative analysis on downscaled climate scenarios for headwater catchment of Yellow River using SDS and delta methods. *Acta Meteorologica Sinica*, *65*(4), 653–662.
[28] Yao, S. (2016). *Risk assessment of urban rainstorm disaster—A case study of Beijing-Tianjin-Hebei region* [Master's thesis]. Tsinghua University.
[29] Li, R., Li, Y., & Xu, Y. (2018). Projection of rainstorm and flooding disaster risk in China in the 21st century. *Journal of Arid Meteorology*, *36*(3), 341–352.
[30] Zhang, Y., Wang, C., Liu, K., & Chen, Q. (2015). Applicability of different probability distributions to estimated extreme rainfall. *Geographical Science*, *35*(11), 1460–1467.
[31] Coles, S. (2001). *An Introduction to Statistical Modeling of Extreme Values*. Springer.
[32] Cui, Y., & Liu, T. (2021). Quantitative research on water system heritage of Chengde Mountain Resort based on SWMM. *Chinese Landscape Architecture*, *37*(12), 59–63.
[33] Liang, H., & Li, S. (2022). The construction intensity of rainwater runoff purification facilities in mountainous villages based on SWMM. *Huazhong Architecture*, *40*(5), 108–115.
[34] Sun, Z., Du, Y., & Wang, S. (2024). Hydrological cost-benefit analysis of stormwater management strategy in northern coastal mountain parks. *Landscape Architecture*, *31*(6), 99–105.
[35] Moriasi, D. N., Gitau, M. W., Pai, N., & Daggupati, P. (2015). Hydrologic and water quality models: Performance measures and evaluation criteria. *Transactions of the ASABE*, *58*(6), 1763–1785.
[36] Bohorquez, P., & del Moral-Erencia, J. D. (2017). 100 years of competition between reduction in channel capacity and streamflow during floods in the Guadalquivir River (Southern Spain). *Remote Sensing*, *9*(7), 727.
[37] Li, X., Xu, C., Li, L., Luo, Y., Yang, Q., & Yang, Y. (2019). Evaluation of air temperature of the typical river basin in desert area of Northwest China by the CMIP5 models: A case of the Kaidu-Kongqi River Basin. *Resources Science*, *41*(6), 1141–1153.
[38] Zhai, G. (2024). Living with risk: Building the future of resilient cities. *Landscape Architecture Frontiers*, *12*(1), 88–92.

https://doi.org/10.15302/J-LAF-0-020035 收稿日期 | 2024-10-15 录用日期 | 2025-04-22 中图分类号 | TU986 文献标识码 | A

气候变化情景下山地乡村聚落雨洪风险模拟评估

孙喆[1,*]，贾雨薇[1]，吴其江[1]，蒋家星[1]，郑璐[1]，崔子璇[1]，卢卡·玛丽亚·弗朗西斯科·法布里斯[1,2]

1 北京建筑大学建筑与城市规划学院，北京 100044
2 米兰理工大学建筑、城市规划与建设工程学院，米兰 20133

***通信作者**
地址：北京市西城区展览馆路1号
邮编：100044
邮箱：sunzhe@bucea.edu.cn

摘要

气候变化导致极端气象事件的强度和频度显著提升，对大量山区乡村聚落的水文生态安全造成了较大挑战，因此亟需对未来气候情景下的山区村庄雨洪风险预测开展研究。本研究以北京市永定河流域的山区为例，利用CMIP6数据和Delta统计降尺度方法，对本世纪末SSP126、SSP245、SSP585情景下，重现期为20、50、100年的降雨事件进行预测，并采用SWMM耦合HEC-RAS二维水动力模型，对永定河河道两侧村庄聚落进行淹没模拟。研究结果发现：1）就总体洪涝风险而言，位于清水河下游、永定河峡谷出口段的村庄洪水风险偏高，并且在未来三种气候情景下，淹没面积占比、最大淹没深度，以及村庄淹没数量均显著增加；2）随着SSP路径的辐射强迫值增大，世纪末期淹没面积占比最高增加了8.22%，在未来气候条件下山地聚落的防洪压力显著增大；3）分析空间特征与聚落洪水灾害的相关性结果显示，聚落淹没面积占比与河道平均宽度、弯曲度呈显著负相关，与河道比降及聚落是否紧邻行洪沟呈显著正相关；最大淹没深度与河道平均宽度呈显著负相关，与是否紧邻行洪沟呈显著正相关。本文最后提出应对未来气候变化情景的“重点区域防洪+可持续开发”策略，建议整合上下游各类空间要素资源，以降低未来气候变化对山地聚落造成的雨洪风险。

关键词

气候变化；CMIP6；山地聚落；雨洪风险；永定河流域；空间特征；极端降雨事件

文章亮点

- 采用Delta-GEV模型方法预测未来气候情景下2100年时山区流域村庄的洪水风险
- 随着极端降水的加强，洪水风险呈上升趋势，淹没面积占比最高增加了8.22%
- 通过乡村聚落空间指标量化雨洪风险以支撑韧性规划决策

基金项目

- 北京市属高校教师队伍建设支持计划优秀青年人才培育计划项目“城市蓝绿景观对热岛效应的减缓机制及优化策略研究”（编号：BPHR202203082）
- 国家社会科学基金项目“新旧杂陈的历史街区、古村古镇保护经验研究”（编号：24VWB022）
- 国家自然科学基金项目“山地传统聚落洪涝适灾机理解析与应用研究”（编号：52478039）

编辑 田乐，马锡栋